Microelectronics Journal 50 (2016) 60–65

Contents lists available at ScienceDirect

Microelectronics Journal

journal homepage: www.elsevier.com/locate/mejo

Analytical models for channel potential, threshold voltage, and subthreshold swing of junctionless triple-gate FinFETs

Guangxi Hu *, Shuyan Hu, Jianhua Feng, Ran Liu, Lingli Wang, Lirong Zheng

State Key laboratory of ASIC and system, School of Information Science and Technology, Fudan University, 220 Handan Road, Shanghai 200433, China

ARTICLE INFO

Article history:
Received 7 April 2015
Received in revised form
5 October 2015
Accepted 4 February 2016
Available online 23 February 2016

Keywords:
Semiconductor device
Analytical
MOSFET
Modeling and simulation

ABSTRACT

Analytical models for channel potential, threshold voltage, and subthreshold swing of the short-channel fin-shaped field-effect transistor (FinFET) are obtained. The analytical model results are verified against simulations and good agreements are observed. Analytical expressions for subthreshold swing, drain induced barrier lowering effect, and threshold voltage roll-off characteristics are presented. The explicit expressions for threshold voltage and subthreshold swing make the model useful in the practical applications of the device.

1. Introduction

As the channel length of metal–oxide–semiconductor field-effect transistors (MOSFETs) scales down to the deca-nanometer regimes, short channel effects (SCEs), carrier mobility degradation, and currents tunneling through the extremely thin gate oxide become much more serious [1]. To solve these problems, a new type of MOSFET, the triple-gate FinFET, has been proposed, studied and adapted as a technical solution for the 22 nm technology node and beyond [2–9]. However, as MOSFETs continue to scale down to the nanometer regimes, the fabrication processes of the source/drain (S/D) of the traditional inversion-mode (IM) transistor are rather complicated; the large contact resistances of S/D of the IM transistor degrade the MOSFETs; and the thermal budget of the traditional S/D will be a heavy burden. All these problems will limit the use of the triple-gate FinFETs. To tackle these problems and to improve the device performance, the junctionless (JL) MOSFET was put forward and explored to a great extent [10–17]. Unlike the traditional IM transistor where accepters and donors are doped in the channel and the S/D regions, respectively, a JL transistor is doped with the same type of dopant throughout the channel and S/D regions. Therefore, the fabrication processes are simplified and the S/D contact resistances are decreased.

To facilitate the applications of the device in integrated circuits, analytical models for channel potential, threshold voltage, V_{th}, and subthreshold swing, *SS*, are inevitably needed in the practical use of the device. Lots of theoretical researches have been carried out on the characteristics of drain current, I_{DS}, V_{th}, and *SS* of the JL double-gate (DG) MOSFETs in the literature [18–21]. Explorations on the analytical models of the JL surrounding-gate (SG) or nanowire MOSFETs have been conducted in [22–26]. In our previous work, we obtained the analytical models of V_{th} and *SS* for JL SG transistors [27]. Trevisoli and others investigated the I_{DS} model for triple-gate JL nanowire transistors [28]. They obtained the I_{DS} model based on the approach of adding the solution of the 3-D Laplace equation to the solution of the 2-D Poisson equation, instead of solving the 3-D Poisson equation directly. The analytical expressions for V_{th} and *SS* of the JL FinFET with a short channel are desired in the applications of the device.

In this work, we focus our research on the V_{th} and *SS* of the JL FinFET with a short channel. We solve the 3-D Poisson equation directly and obtain an analytical expression for channel potential. Then, we achieve the analytical expression for V_{th} based on the new definition we put forward in our previous work [27]. After that, analytical expressions for *SS*, drain induced barrier lowering effect (DIBL) and V_{th} roll-off characteristics are obtained.

2. Analytical model

The sketches of the JL FinFET similar to those in [8] are shown in Fig. 1(a) and (b). The Cartesian axes of *x*, *y*, and *z* are along the channel length, width, and height directions, respectively. The channel material of the device is heavily n-doped silicon. The channel is surrounded with a very thin oxide layer and the oxide is

* Corresponding author.
E-mail address: gxhu@fudan.edu.cn (G. Hu).

http://dx.doi.org/10.1016/j.mejo.2016.02.003
0026-2692/

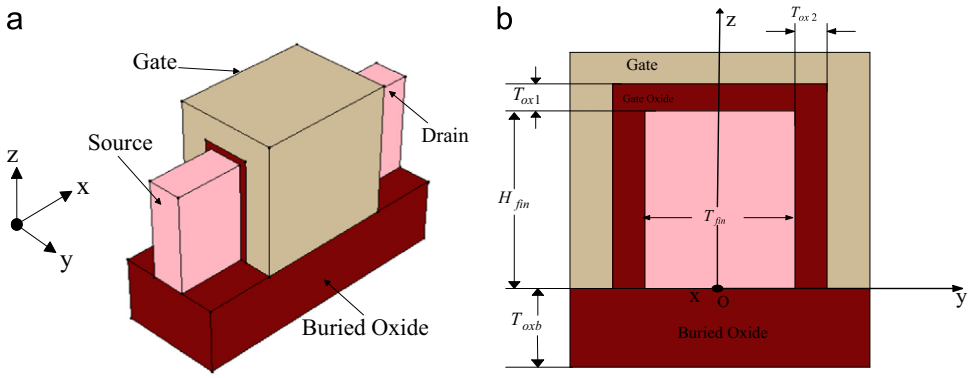

Fig. 1. (a) Bird's eye view of a FinFET. (b) Cross section view of a FinFET.

then enclosed with a fin-shaped gate, which can either be a metal or a heavily doped polysilicon.

The Poisson equation in the channel is

$$\frac{\partial^2\phi}{\partial x^2}+\frac{\partial^2\phi}{\partial y^2}+\frac{\partial^2\phi}{\partial z^2}=-\frac{qN_D}{\varepsilon_{si}}\left[1-\exp\left(\frac{\phi-V}{V_t}\right)\right], \tag{1}$$

where ϕ is electric potential, N_D the doping density, and ε_{si} the permittivity of silicon. $V_t=k_BT/q$ is thermal voltage and V is the quasi-Fermi potential. q, k_B, and T have their usual meanings.

2.1. Electric potential in the channel

In this work, the voltage at the source end is set to be the reference, V_R. Similar to the treatment used in [2,3,8], the boundary conditions of the device can be simplified as follows:

$$\phi(0,y,z)=V_R \tag{2a}$$

$$\phi(L,y,z)=V_R+V_{DS}, \tag{2b}$$

$$\phi(x,T_{eff}/2,z)=V_{GS}-V_{FB}, \tag{2c}$$

$$\phi(x,-T_{eff}/2,z)=V_{GS}-V_{FB}, \tag{2d}$$

$$\phi(x,y,H_{eff})=V_{GS}-V_{FB}, \tag{2e}$$

$$\left.\frac{\partial\phi}{\partial z}\right|_{z=0}=0 \tag{2f}$$

where V_{DS} is the drain bias, V_{GS} the gate bias, V_{FB} the flat-band voltage, and L the gate length. T_{eff} and H_{eff} are effective thickness and effective height of the channel, defined as [2,3]

$$T_{eff}=\sqrt{T_{fin}\left(T_{fin}+4T_{ox2}\varepsilon_{si}/\varepsilon_{ox}\right)}, \tag{3a}$$

$$H_{eff}=\sqrt{H_{fin}\left(H_{fin}+2T_{ox1}\varepsilon_{si}/\varepsilon_{ox}\right)}, \tag{3b}$$

where T_{ox1}, and T_{ox2} are the oxide thicknesses shown in Fig. 1(b), and we assume $T_{ox1}=T_{ox2}=T_{OX}$ in this work. H_{fin}, and T_{fin} are the channel height and channel thickness, respectively. ε_{ox} is the permittivity of the oxide.

From (2f), the bottom boundary condition could be replaced with the following equation [3]

$$\phi(x,y,-H_{eff})=V_{GS}-V_{FB}. \tag{4}$$

It is hard to obtain an analytic solution of potential ϕ in (1). Different from the traditional IM FinFET, the JL FinFET will be turned on in the partially depleted region, and turned off in the fully depleted region [21,25,27]. Similar to the treatment used in [25,27], a full depletion approximation is used, the exponential term in (1) can be ignored in the subthreshold region, and (1) is simplified to:

$$\frac{\partial^2\phi}{\partial x^2}+\frac{\partial^2\phi}{\partial y^2}+\frac{\partial^2\phi}{\partial z^2}=-\frac{qN_D}{\varepsilon_{si}}. \tag{5}$$

With boundary conditions (2a) and (2b), the electric potential along the channel length direction (x) can be described by a summation of series [8,29,30], then, analytic solution for (5) can be obtained

$$\phi(x,y,z)=V_R+\frac{V_{DS}}{L}x+\sum_{n=1}^{\infty}A_n(y,z)\sin\left(\frac{n\pi}{L}x\right) \tag{6}$$

As shown in the Appendix A, $A_n(y,z)$ is given by

$$A_n(y,z)=G_n(y,z)+\varphi_n, \tag{7}$$

$$\begin{aligned}
&\text{where } G_n(y,z)=\sum_m\sum_l g_{ml}(n)\cos\left[\frac{(m-0.5)\pi}{t}y\right]\cos\left[\frac{(l-0.5)\pi}{h}z\right]\\
&g_{ml}(n)=\frac{(-1)^{m+l+1}4(d_n+k_n^2\varphi_n)}{(m-0.5)(l-0.5)\pi^4\left[(m-0.5)^2/t^2+(l-0.5)^2/h^2+n^2/L^2\right]},\\
&\varphi_n=\frac{2}{n\pi}\left\{(V_{GS}-V_{FB}-V_R)\left[1-(-1)^n\right]+V_{DS}(-1)^n\right\}\\
&k_n=n\pi/L,\ d_n=\frac{2qN_D}{n\pi\varepsilon_{si}}\left[(-1)^n-1\right]\\
&t=T_{eff}/2,\ h=H_{eff}
\end{aligned} \tag{8}$$

m, n, and l are all positive integers.

2.2. Threshold voltage

Similar to the definition used in [25,27], the threshold voltage in this paper is defined as the voltage applied to the gate to make the whole channel in full depletion, which means the mobile charges can be neglected. Exactly speaking, however, the mobile charge density varies in the channel as a function of the electric potential. We choose a location where the electric potential of the average value, ϕ_{ave}. Generally, for the JL FinFETs, $V_{GS}<V_{FB}$, then along the y and z directions, the electric potential will be the highest at the location $y=0$ and $z=0$. So we choose the average potential place at the location: $x=x_{min}, y=0, z=0$, which means

$$\varphi_{ave}=\varphi(x_{min},0,0), \tag{9}$$

where $x=x_{min}$ is the location the electric potential reaches the minimum along the x direction, it can be approximated as [2,4]:

$$x_{min}=\frac{L}{2}-\frac{1}{2\pi}\left(\frac{1}{T_{eff}^2}+\frac{0.5}{H_{eff}^2}\right)^{-1/2}\ln\left(1+V_{DS}/V_R\right). \tag{10}$$

If the following equation holds true,

$$\varphi(x_{min},0,0)-V=-2V_t, \tag{11}$$

the exponential term in (1) is then negligibly small and the channel can be considered as in full depletion condition, and,

therefore, the voltage applied to the gate now is defined as threshold voltage. We proposed this definition in [27] and we named it as the φ_{min} method.

To obtain an analytic expression for V_{th}, we use the dominant-term approximation, which means we keep only the largest term for every summation in the expression of $\varphi(x_{min},0,0)$, i.e., $n=m=l=1$ is used. Then, using a constant quasi-Fermi potential, $V=V_R$, we obtain the V_{th} from (11) as following

$$V_{th}=V_{FB}+V_R+\frac{1}{2}V_{DS}-\left(\frac{\pi}{4}\right)\frac{B-64d_1}{A-64k_1^2}, \tag{12}$$

where

$$A=\pi^4\left(1/t^2+1/h^2+4/L^2\right),$$

$$B=A\left[2V_t+V_{DS}(x_{min}/L)\right]/\ \sin\left(\pi x_{min}/L\right),$$

$$d_1=-(4qN_D)/(\pi\varepsilon_{si}),$$

$$k_1=\pi/L.$$

For the device with a long channel, $x_{min}=L/2$, V_{th} can be expressed as

$$V_{th}^{L}\approx V_{FB}+V_R-\left(\frac{64}{\pi^4}\right)\left(\frac{qN_D}{\varepsilon_{si}}\right)\frac{1}{\left(1/t^2+1/h^2\right)}. \tag{13}$$

2.3. DIBL effect

DIBL effect, the variation of V_{th} with respect to V_{DS}, can be obtained from (12). For simplicity, we ignore the variation of x_{min} with respect to V_{DS}, and then

$$DIBL=\frac{\partial V_{th}}{\partial V_{DS}}\approx\frac{1}{2}-\frac{\pi}{4}\frac{Ax_{min}}{L\ \sin\left(\pi x_{min}/L\right)\left(A-64k_1^2\right)}. \tag{14}$$

2.4. Threshold voltage roll-off characteristics

Threshold voltage roll-off Characteristics is defined as the variation of V_{th} with respect to channel length, L. Since x_{min}/L can be treated as a constant, V_{th} roll-off, V_{th}^{R-O} is approximated as

$$V_{th}^{R-O}=\frac{\partial V_{th}}{\partial L}\approx\left(\frac{2\pi^3}{L^3}\right)\frac{\pi^2\left(A-64k_1^2\right)/\ \sin\left(\pi x_{min}/L\right)+(B-64d_1)\left(16-\pi^2\right)}{\left(A-64k_1^2\right)^2} \tag{15}$$

2.5. Subthreshold swing

The definition of subthreshold swing is: $SS=\partial V_{GS}/\partial\log_{10}I_{DS}$. Assuming the subthreshold drain-to-source current, I_{DS}, is proportional to $\exp(\phi_{ave}/V_t)$ [27,30,31], then we can obtain SS from $SS=2.3V_t\left[\partial\phi_{ave}/\partial V_{GS}\right]^{-1}$ as

$$SS=\frac{1.81V_t}{\sin\left(\frac{\pi x_{min}}{L}\right)\left(1-\frac{64}{\pi^2(L^2/t^2+L^2/h^2+4)}\right)}. \tag{16}$$

3. Verification and results

Our models are verified against a simulation tool, Sentaurus [32]. In the simulation, hydrodynamic model is used. Trap assisted Auger processes and tunneling, as well as band to band tunneling is included. The dependencies of carriers' mobility on the doping concentration, temperature, normal and high electric field, are considered.

Table 1
Parameter values used in the model.

Parameter	Description	Value
T_{OX}	Thickness of the oxide	1.5 nm
N_D	Channel doping density	10^{19} cm^{-3}
μ	Electron mobility	300 cm^2/V s
V_R	Reference voltage	0.52 V
T	Temperature	300 K

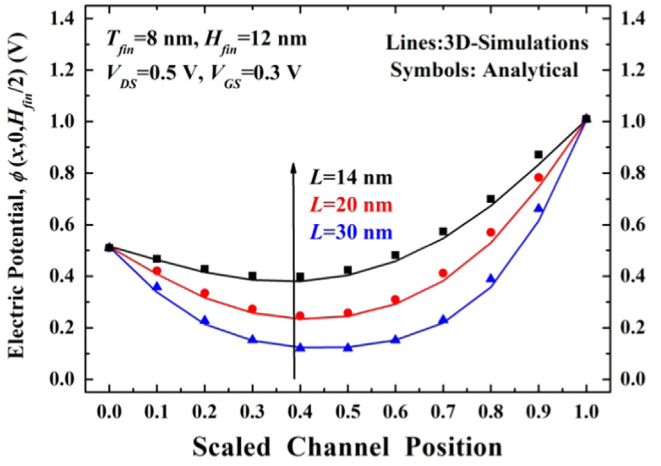

Fig. 2. Electric potential at the channel center versus scaled channel position. Lines are simulation results while symbols are analytical results. Good agreements are observed.

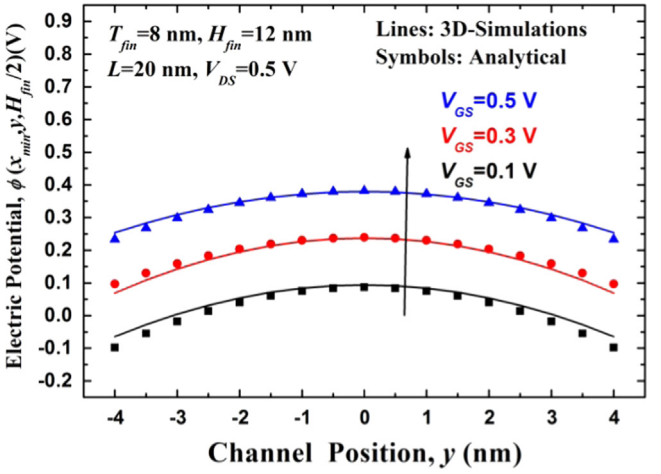

Fig. 3. Electric potential along width direction. Lines are simulation results while symbols are analytical results.

In the simulation, a heavily doped p^+ polysilicon is chosen for the gate. Unless stated otherwise, the parameter values used are shown in Table 1.

Fig. 2 shows the electrical potential along the channel length direction. We notice that the potential reaches a minimum near the middle of the channel length, which is consistent with Eq. (8). The solid lines are simulation results while the symbols are analytical results, good agreements are observed. The black squares, red circles, and blue triangles are for the devices with $L=14$, 20, and 30 nm, respectively.

Fig. 3 presents the electric potential along the channel width direction. The electric potential gets to the maximum in the middle of the channel width, $y=0$. Lines are simulation results while symbols are analytical results, and they match very well.

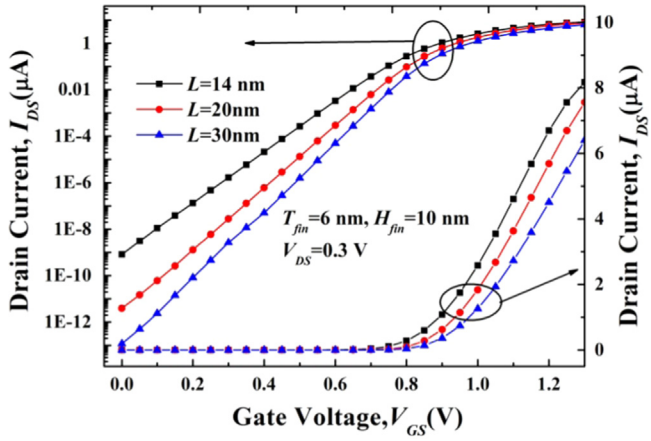

Fig. 4. Simulation results for drain current versus gate bias for different channel lengths. The left is for logarithmic scale, while the right is for linear scale.

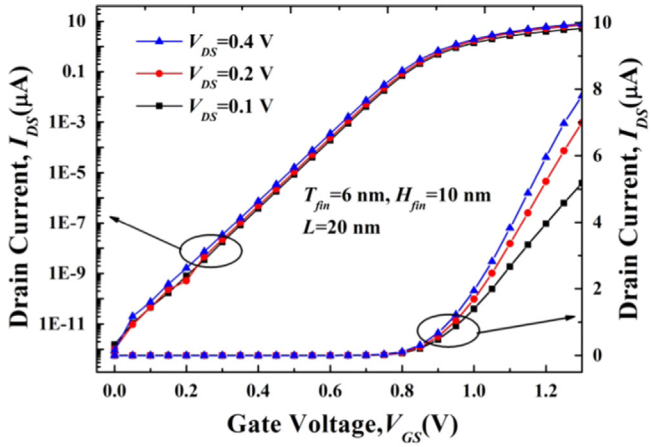

Fig. 5. Simulation results for drain current versus gate bias for different drain biases. A turning point is noticed around the gate bias of 0.85 V. The left and the right are for logarithmic and linear scales, respectively.

Figs. 4 and 5 cshow the drain current characteristics. The definition of V_{th} presented in (12) is consistent with drain current characteristics. It is noted that each drain current seems to have a turning point at a gate bias of about 0.85 V, which corresponds to the threshold voltage. The same results can be expected from Eq. (12).

In the literature [25,27], V_{th} was defined as gate voltage at which the ratio of transconductance to the drain current, g_m/I_{DS}, dropped to half of its maximum value, we call this definition the g_m/I_{DS}method. Fig. 6 presents the simulated ratio of g_m/I_{DS}. It can be seen that for a device with L=20 nm, the threshold voltage is 0.85 V. This confirms that our V_{th} definition ($\phi_{\min}$ method) is consistent with that of the g_m/I_{DS} method.

Fig. 7 characterizes the threshold voltage roll-off with the down scaling of channel length. Up and down triangles are simulation results with φ_{min} method for V_{DS}=0.1 V and 0.5 V, respectively. Squares and circles are those with g_m/I_{DS} method for V_{DS}=0.1 V and 0.5 V, respectively. Solid line and dashed line are analytical results for V_{DS}=0.1 V and 0.5 V, respectively. V_{th} decreases with the reduction of L, and/or with the increase of V_{DS}, and these behaviors are similar to those of its counterpart, IM device [33].

We notice that model results deviate from simulation results a little, especially when the channel length is short. The differences may stem from the fully depletion approximation and other approximations have been used, and g_m/I_{DS} method usually underestimates V_{th} [27].

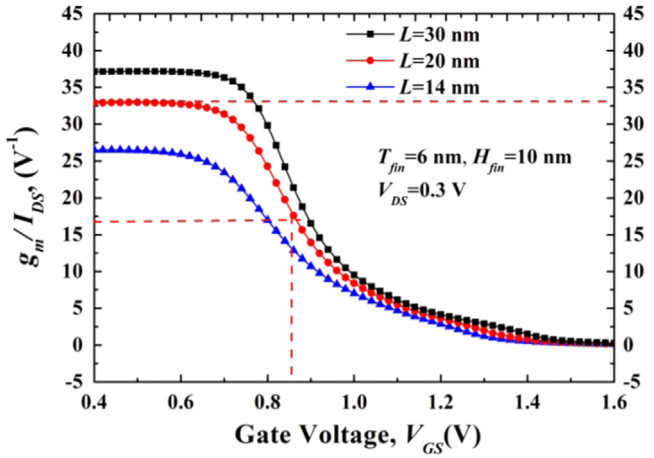

Fig. 6. Simulated results for the ratio, g_m/I_{DS}, versus gate bias. For the device with L=20 nm, half of the maximum value of the ratio g_m/I_{DS} corresponds to a gate voltage of 0.85 V, which is V_{th}.

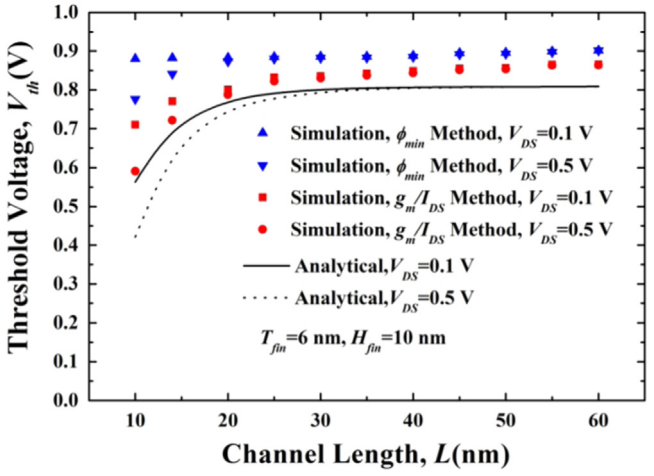

Fig. 7. Threshold voltage roll-off characteristics. Symbols are simulation results, up and down triangles are results with φ_{min} method, while squares and circles are results with g_m/I_{DS} method. Lines are for analytical results.

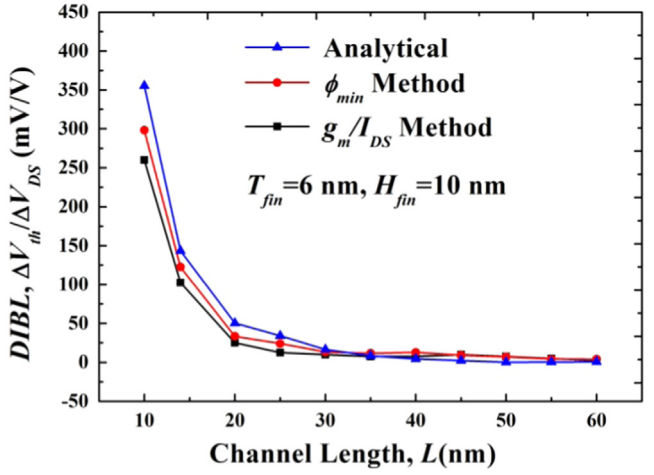

Fig. 8. DIBL effects versus channel length. Solid line with triangles, with circles, and with squares are for φ_{min} method, g_m/I_{DS} method, and analytical, respectively.

Fig. 8 presents the DIBL effects. Blue line with triangles is for analytical results, which are obtained from Eq. (14). Red line with circles is for simulation result where V_{th} is extracted with φ_{min}

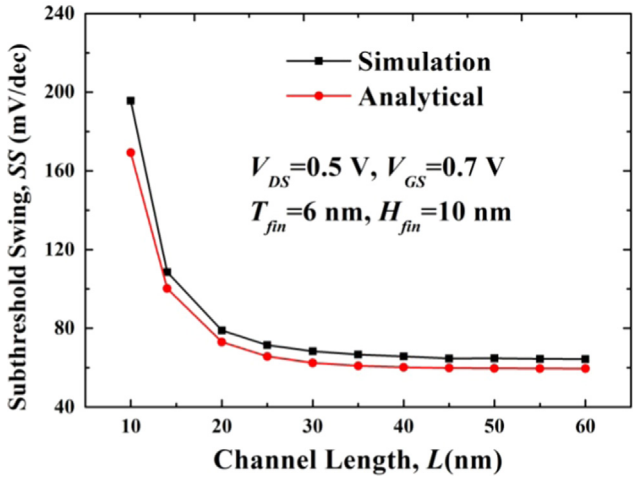

Fig. 9. Subthreshold swing versus channel length. Black line with squares and red line with circles are for simulated and analytical results, respectively. (For interpretation of the references to color in this figure legend, the reader is referred to the web version of this article.)

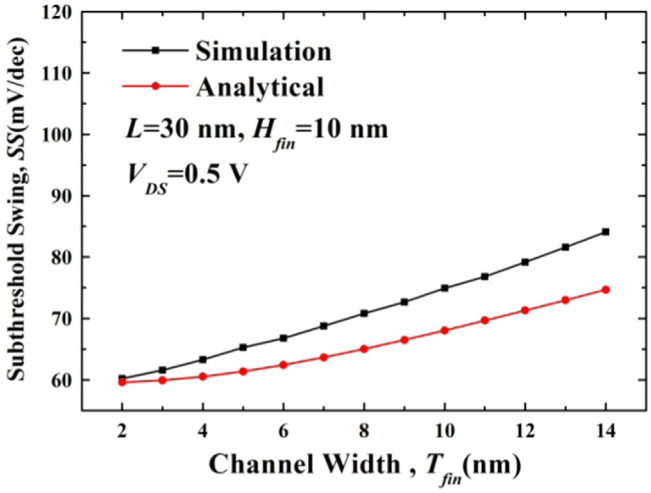

Fig. 10. Subthreshold swing versus channel width. Black line with squares and red line with circles are for simulated and analytical results, respectively. (For interpretation of the references to color in this figure legend, the reader is referred to the web version of this article.)

method. Black line with squares is for simulated result where V_{th} is obtained with g_m/I_{DS} method. When the channel length is smaller than 20 nm, the DIBL effects will be very serious.

Figs. 9 and 10 reveal the subthreshold swing behaviors of the device. Black line with squares and red line with circles are for simulated and analytical results, respectively. Analytical results are obtained from Eq. (16). It is noted that, subthreshold swing will get worse with the reduction of channel length, and/or with the increase of channel width. As the channel length reduces, short channel effect will deteriorate the subthreshold swing. When the channel width increases, it will be more difficult for the gate to control the channel, therefore, the subthreshold swing of the device becomes worse.

One point should be noted is that, in Fig. 10, the differences between analytical results and simulation results increase with the increase of channel width, T_{fin}, this is attributed to the dominant-term approximation has been used.

4. Discussion and concluding remarks

An analytical expression for channel potential is obtained by solving a 3-D Poisson equation without gradual channel approximation. Based on the potential model, analytical expressions for V_{th}, DIBL effect, V_{th} roll-off characteristics, and SS are presented. The proposed models have been verified against the commercial device simulator and good agreements are observed. The explicit expressions for V_{th} and SS make the models useful in the applications of the device.

Model and simulation results suggest that, for the JL FinFET, we have the following simulation and design insights:

(1) For the device with a long channel (>40 nm), V_{th} can be obtained with Eq. (13) very quickly.
(2) When the channel length is small (<15 nm), the V_{th} roll-off effect will be significant. One should be careful with the use of a device with a very short channel.
(3) The subthreshold swing increases with the reduction of channel length, and/or with the increase of channel width. To obtain a desirable subthreshold swing, one should make a trade-off between channel length and channel width.
(4) For fast simulations, the location at which electric potential is minimum along the x direction, x_{min}, can be dealt with a fitting parameter instead of using (10). It can be approximated with $0.4L$, which has minor effect on the results.

Acknowledgment

Precious support from Shanghai Science Foundation under Grant No. 14ZR1402600 is appreciated. This work is supported in part by National Natural Science Foundation of China (Grant No. 61571137).

Appendix A. The derivation of channel potential

Substituting (6) into (5), we find the coefficients, $A_n(y,z)$, are determined by

$$\sum_{n=1}^{\infty}\left[\frac{\partial^2 A_n(y,z)}{\partial y^2}+\frac{\partial^2 A_n(y,z)}{\partial z^2}-k_n^2 A_n(y,z)\right]\sin\left(\frac{n\pi}{L}x\right)=-\frac{qN_D}{\varepsilon_{si}}, \tag{A1}$$

Using Fourier series expansion, we obtain from (A1)

$$\frac{\partial^2 A_n(y,z)}{\partial y^2}+\frac{\partial^2 A_n(y,z)}{\partial z^2}-k_n^2 A_n(y,z)=d_n \tag{A2}$$

where d_n is given by

$$d_n=\frac{2qN_D}{n\pi\varepsilon_{si}}[(-1)^n-1] \tag{A3}$$

Substituting (6) into (2c), (2d), (2e), and (4), the boundary conditions can be described as

$$\sum_{n=1}^{\infty}A_n\left(\tfrac{T_{eff}}{2},z\right)\sin\left(\tfrac{n\pi}{L}x\right)=V_{GS}-V_{FB}-V_R-\tfrac{V_{DS}}{L}x, \tag{A4a}$$

$$\sum_{n=1}^{\infty}A_n\left(-\tfrac{T_{eff}}{2},z\right)\sin\left(\tfrac{n\pi}{L}x\right)=V_{GS}-V_{FB}-V_R-\tfrac{V_{DS}}{L}x, \tag{A4b}$$

$$\sum_{n=1}^{\infty}A_n\left(y,H_{eff}\right)\sin\left(\tfrac{n\pi}{L}x\right)=V_{GS}-V_{FB}-V_R-\tfrac{V_{DS}}{L}x, \tag{A4c}$$

$$\sum_{n=1}^{\infty}A_n\left(y,-H_{eff}\right)\sin\left(\tfrac{n\pi}{L}x\right)=V_{GS}-V_{FB}-V_R-\tfrac{V_{DS}}{L}x. \tag{A4d}$$

Using Fourier series expansion, we obtain

$$A_n(T_{eff}/2,z)\quad=A_n(-T_{eff}/2,z)=\varphi_n, \tag{A5a}$$

$$A_n(y,H_{eff})=A_n(y,-H_{eff})=\varphi_n, \tag{A5b}$$

where

$$\varphi_n = \frac{2}{n\pi}\left[(V_{GS}-V_{FB}-V_R)[1-(-1)^n]+V_{DS}(-1)^n\right]. \quad \text{(A6)}$$

Assuming

$$A_n(y,z) = G_n(y,z)+\varphi_n \quad \text{(A7)}$$

Substituting (A7) into (A2), we obtain

$$\frac{\partial^2 G_n(y,z)}{\partial y^2}+\frac{\partial^2 G_n(y,z)}{\partial z^2}-k_n^2 G_n(y,z) = d_n + {k_n}^2\varphi_n \quad \text{(A8)}$$

Now that $G_n(y,z)$are zero on the 4 boundaries set by, $y=\pm T_{eff}/2$, and $z=\pm H_{eff}$, the solution of $G_n(y,z)$ can be expressed as

$$G_n(y,z) = \sum_{m,l} g_{ml}(n)\cos\left(\frac{(m-0.5)\pi}{t}y\right)\cos\left(\frac{(l-0.5)\pi}{h}z\right) \quad \text{(A9)}$$

The coefficients, $g_{ml}(n)$, can be obtained by substituting (A9) into (A8), leading to

$$g_{ml}(n) = \frac{(-1)^{m+l+1}4(d_n+k_n^2\varphi_n)}{(m-0.5)(l-0.5)\pi^4\left[(m-0.5)^2/t^2+(l-0.5)^2/h^2+n^2/L^2\right]} \quad \text{(A10)}$$

At last, the analytic expression for channel potential is obtained

$$\phi(x,y,z) = V_R+\frac{V_{DS}}{L}x+\sum_{n=1}^{\infty}\left[G_n(y,z)+\varphi_n\right]\sin\left(\frac{n\pi}{L}x\right) \quad \text{(A11)}$$

where φ_n and $G_n(y,z)$ are given by (A6) and (A9), respectively.

References

[1] Z. Ding, G. Hu, R. Liu, L. Wang, S. Hu, X. Zhou, Analytical models for electric potential, threshold voltage and drain current of long-channel junctionless double-gate transistors, J. Korean Phys. Soc. 62 (8) (2003) 1188–1193.

[2] G. Pei, J. Kedzierski, P. Oldiges, M. Ieong, E.C.C. Kan, FinFET design considerations based on 3-D simulation and analytical modeling, IEEE Trans. Electron Devices 49 (8) (2002) 1411–1419.

[3] W. Yang, Z. Yu, L. Tian, Scaling theory for FinFETs based on 3-D effects investigation, IEEE Trans. Electron Devices 54 (5) (2007) 1140–1147.

[4] R. Ritzenthaler, F. Lime, O. Faynot, S. Cristoloveanu, 3D analytical modeling of subthreshold characteristics in vertical Multiple-gate FinFET transistors, Solid-State Electron. 65–66 (2011) 94–102.

[5] A. Kloes, M. Schwarz, T. Holtij, MOS^3: a new physics-based explicit compact model for lightly doped short-channel triple-gate SOI MOSFETs, IEEE Trans. Electron Devices 59 (2) (2012) 349–359.

[6] N. Fasarakis, A. Tsormpatzoglou, D.H. Tassis, I. Pappas, K. Papathanasiou, M. Bucher, G. Ghibaudo, C.A. Dimitriadis, Compact model of drain current in short-channel triple-gate FinFETs, IEEE Trans. Electron Devices 59 (7) (2012) 1891–1898.

[7] H.A.E. Hamid, J.R. Guitart, V. Kilchytska, D. Flandre, B. Iñiguez, A 3-D analytical physically based model for the subthreshold swing in undoped trigate FinFETs, IEEE Trans. Electron Devices 54 (9) (2007) 2487–2496.

[8] P. Xiang, E. Gu, G. Hu, R. Liu, L. Wang, X. Zhou, Analytical models for channel potential, drain current, and subthreshold swing of short channel triple-gate FinFETs, Far East J. Electron. Commun. 12 (1) (2014) 39–48.

[9] M. Saremi, A. Afzali-Kusha, S. Mohammadi, Ground plane fin-shaped field effect transistor (GP-FinFET): a FinFET for low leakage power circuits, Microelectron. Eng. 95 (2012) 74–82.

[10] C.-W. Lee, A. Afzalian, N.D. Akhavan, R. Yan, I. Ferain, J.-P. Colinge, Junctionless multigate field-effect transistor, Appl. Phys. Lett. 94 (5) (2009) 053511-1–053511-2.

[11] J.-P. Colinge, C.-W. Lee, A. Afzalian, N.D. Akhavan, R. Yan, I. Ferain, et al., Nanowire transistors without junctions, Nat. Nanotechnol. 5 (3) (2010) 225–229.

[12] J.-P. Colinge, C.-W. Lee, I. Ferain, N.D. Akhavan, R. Yan, P. Razavi, et al., Reduced electric field in junctionless transistors, Appl. Phys. Lett. 96 (7) (2010) 073510-1–073510-3.

[13] C.-W. Lee, A.N. Nazarov, I. Ferain, N.D. Akhavan, R. Yan, P. Razavi, R. Yu, R. T. Doria, J.-P. Colinge, Low subthreshold slope in junctionless multigate transistors, Appl. Phys. Lett. 96 (10) (2010) 102106-1–102106-3.

[14] S.J. Park, D.-Y. Jeon, L. Montès, S. Barraud, G.-T. Kim, G. Ghibaudo, Back biasing effects in tri-gate junctionless transistors, Solid-State Electron. 87 (2013) 74–79.

[15] D.-Y. Jeon, S.J. Park, M. Mouis, S. Barraud, G.-T. Kim, G. Ghibaudo, Low-temperature electrical characterization of junctionless transistors, Solid-State Electron. 80 (2013) 135–141.

[16] T.K. Kim, D.H. Kim, Y.G. Yoon, et al., First demonstration of junctionless accumulation-mode bulk FinFETs with robust junction isolation, IEEE Electron Device Lett. 34 (12) (2013) 1479–1481.

[17] R. Rios, A. Cappellani, M. Armstrong, A. Budrevich, H. Gomez, R. Pai, N. Rahhal-orabi, K. Kuhn, Comparison of junctionless and conventional trigate transistors with Lg down to 26 nm, IEEE Electron Device Lett. 32 (9) (2011) 1170–1172.

[18] Y. Taur, H.-P. Chen, W. Wang, S.-H. Lo, C. Wann, On-off charge–voltage characteristics and dopant number fluctuation effects in junctionless double-gate MOSFETs, IEEE Trans. Electron Devices 59 (3) (2012) 863–866.

[19] B.C. Paz, F. Ávila-Herrera, A. Cerdeira, M.A. Pavanello, Double-gate junctionless transistor model including short-channel effects, Semicond. Sci. Technol. 30 (2015) 055011-1–055011-11.

[20] A. Cerdeira, M. Estrada, B. Iniguez, R.D. Trevisoli, R.T. Doria, M. de Souza, M. A. Pavanello, Charge-based continuous model for long-channel symmetric double-gate junctionless transistors, Solid-State Electron. 85 (2013) 59–63.

[21] J.P. Duarte, S.-J. Choi, D.-I. Moon, Y.-K. Choi, Simple analytical bulk current model for long-channel double-gate junctionless transistors, IEEE Electron Device Lett. 32 (6) (2011) 704–706.

[22] J.P. Duarte, S.-J. Choi, D.-I. Moon, Y.-K. Choi, A nonpiecewise model for long-channel junctionless cylindrical nanowire FETs, IEEE Electron Device Lett. 33 (2) (2012) 155–157.

[23] S.-J. Choi, D.-I. Moon, S. Kim, J.P. Duarte, Y.-K. Choi, Sensitivity of threshold voltage to nanowire width variation in junctionless transistors, IEEE Electron Device Lett. 32 (2) (2011) 125–127.

[24] R.D. Trevisoli, R.T. Doria, M. de Souza, M.A. Pavanello, A physically-based threshold voltage definition, extraction and analytical model for junctionless nanowire transistors, Solid-State Electron. 90 (2013) 12–17.

[25] R.D. Trevisoli, R.T. Doria, M. de Souza, M.A. Pavanello, Threshold voltage in junctionless nanowire transistors, Semicond. Sci. Technol. 26 (10) (2011) 105009.

[26] A. Gnudi, S. Reggiani, E. Gnani, G. Baccarani, Analysis of threshold voltage variability due to random dopant fluctuations in junctionless FETs, IEEE Electron Device Lett. 33 (3) (2012) 336–338.

[27] G. Hu, P. Xiang, Z. Ding, R. Liu, L. Wang, T.-A. Tang, Analytical models for electric potential, threshold voltage, and subthreshold swing of junctionless surrounding-gate transistors, IEEE Trans. Electron Devices 61 (3) (2014) 688–695.

[28] R.D. Trevisoli, R.T. Doria, M. de Souza, S. Das, I. Ferain, M.A. Pavanello, Surface-potential-based drain current analytical model for triple-gate junctionless nanowire transistors, IEEE Trans. Electron Devices 59 (12) (2012) 3510–3518.

[29] G.-X. Hu, R. Liu, T.-A. Tang, S.-J. Ding, L.-L. Wang, Theory of short-channel surrounding-gate metal-oxide- semiconductor field-effect-transistors, Jpn. J. Appl. Phys. 46 (4A) (2007) 1437–1440.

[30] Z. Ding, G. Hu, J. Gu, R. Liu, L. Wang, T. Tang, An analytic model for channel potential and subthreshold swing of the symmetric and asymmetric double-gate MOSFETs, Microelectron. J. 42 (3) (2011) 515–519.

[31] B. Ray, S. Mahapatra, Modeling of channel potential and subthreshold slope of symmetric double-gate transistor, IEEE Trans. Electron Devices 56 (2) (2009) 260–266.

[32] Sentaurus Device User Guide, Version I−2013.12 (Synopsys Inc., 2013).

[33] Y. Taur, T.H. Ning, Fundamentals of Modern VLSI Devices, Cambridge Univ. Press, Cambridge, 1998.